Laminar free convection from an elliptic tube placed in a Micropolar fluid with vertical plate as a special case

الحمل الحر الرقائقى علي سطح أنبوب بيضاوي في مائع ميكروبولي ودراسة اللوح الراسي كحالة خاصة

Mahfouz F. M.

Mechanical Power Department, Faculty of Engineering, Menoufia University, Shebin El-kom, Egypt

في هذا البحث تم دراسة الحمل الحر من انبوب بيضاوي ساخن موضوع افقيا في مائع ميكروبولي بحيث يكون محوره الاكبر راسيا .ولقد تم حل المعادلات الحاكمة للكتلة ومعدلات كميات الحركة الخطية والدورانية وكذلك الطاقة ،استخدام طريقة عددية دقيقة .والعوامل المتحكمة في هذه الدراسة بالاضافة الي ثوابت المائع الميكروبولي ,هي رقم رايلي ورقم برانتل ونسبة المحور الاصغر الي المحور الاكبر لمقطع البيضاوي .وثوابت المائع هي اللزوجة الدوامية وكثافة القصور المغزلي المتناهي في الصغر وكذلك التدرج الدوراني للزوجة .ولقد تمت الدراسة عند قيمتين لنسبة المحاور وهما 0.5 و 0.025 وهذه الاخيرة تمثل تقريب لحالة اللوح الراسى المستوي .وقد اظهرت نتائج الحمل الحرمن اللوح الراسى الموضوع في مائع نيوتونى (وهو حالة خاصة من المائع الميكروبولي) توافقا ممتازا مع الابحاث السابقة .واظهرت الدراسة عموما ان اللزوجة الدوامية هي اهم ثوابت المائع تاثيرا علي الحمل الحر حيث اظهرت الدراسة انه كلما زادت اللزوجة الدوامية كلما قلت معدلات انتقال الحرارة بالحمل.

Abstract: - In this paper laminar free convection heat transfer from a horizontal isothermal elliptic tube placed in a micropolar fluid with its major axis vertical is investigated. The governing equations based on the conservation of mass, linear momentum, angular momentum and energy are numerically solved using the Fourier Spectral method. The main controlling parameters, beside the material parameters of the micropolar fluid, are the Rayleigh number, the Prandtl number and the elliptic section axis ratio The micropolar fluid parameters are the vortex viscosity, micro-inertia density and spin gradient viscosity. The results, which were obtained for a range of these parameters, were carried out at two axis ratios of 0.5 and 0.025. The axis ratio of 0.025 approximates the geometry of the special case of vertical flat plate. The results for vertical plate placed in Newtonian fluid are compared with the relevant results in the literature and very good agreement was obtained. The study has shown that the vortex viscosity is the most influencing material parameter on heat transfer rate. The study showed that as the vortex viscosity increases the heat transfer rate decreases.

Keywords: Micropolar fluid – free convectioon - microrotation - elliptic tube

1. Introduction

The theory of micropolar fluids has been proposed by Eringen [1]. In this theory the microscopic effects arising from local structure and micromotions of the fluid elements are taken into account. Such fluids can support surface and body couples which are not present in the theory of Newtonian fluids. Micropolar fluids are believed to be successful in describing the behavior of

Accepted November 27, 2005.

exotic lubricants, polymeric fluids, liquid crystals, animal blood, suspension solutions and heterogeneous mixtures such as ferro liquids, most slurries and some liquids with polymer additives. Eringen [2] further extended the micropolar fluid theory to include the thermal effects.

The problem of the buoyancy driven fluid flow adjacent to cylindrical body has long received great attention of the researchers, for it represents a fundamental problem as well as it has many practical applications. These applications include nuclear reactors, heat exchangers, hot wires, cooling of electronic devices, steam pipes and many others. Special interest has been paid to the cylindrical tube of elliptic cross-section due to its flexibility to assume a number of elliptic sections beside the two special extreme cases of circular cylinder (when axis ratio is one) and flat plate when axis ratio is zero) . The axis ratio is the ratio of minor axis to major axis of the ellipse. The works [3-6] have considered the problem of natural convection from elliptic tubes to surrounding Newtonian fluids.

Most of the aforementioned studies have mainly considered the approximate solutions based on simplified boundary layer equations. Such solutions neglect the diffusion (momentum and thermal) in main flow direction which definitely results in inaccuracy in the simulation especially for the low velocity buoyancy driven flow where the diffusion in the flow direction is significant. Badr and Shamsher [7] and Badr [8] have solved the full governing equations to analyze the natural convection from elliptic tubes placed in Newtonian fluids. Badr and Shamsher [7] considered the case of the tube major axis vertical while Badr [8] considered the case of tube at different orientations.

Previous studies of convective heat transfer in micropolar fluids have focused mainly on relatively simple geometry such as flat plates, circular cylinders and simple curved surfaces [9-14]. Most of these studies were mainly related to forced convection problems and/or were based on the numerical solution of simplified (boundary layer) governing equations. There were only a few attempts to investigate the case of natural convection from an elliptic cylinder placed in a micropolar fluid. Among these attempts were those made by Bhattacharyya and Pop [15] and Mahfouz [16]. Bhattacharyya and Pop solved the boundary layer equations to investigate the steady natural convection from an isothermal elliptic tube with its major axis either horizontal or vertical. They presented results for local Nusselt number along with velocity and temperature fields. While Mahfouz solved the full governing equation without boundary layer simplifications to investigate the transient natural convection from an isothermal elliptic tube with its major axis horizontal.

The purpose of this study is to investigate the case of natural convection from elliptic tube with major axis vertical and placed in a micropolar fluid with emphasis on the special case of vertical plate. Attention will be paid to this latter case for two reasons. The first is that it would be a good model problem for testing the accuracy of the method of solution in case of Newtonian fluid. The second it would be convenient herein to provide results for this case which in the author belief has been given scarce or even no attention in case of micropolar fluids.

Nomenclature

a	length of semi-major axis
Ar	axis ratio (=b/a)
b	length of semi-minor axis
c	ellipse eccentricity $(=\sqrt{1-Ar^2})$
f_n	Fourier coefficient
F_b	buoyancy force
g	gravitational acceleration
g_n	Fourier coefficient
H	Jacobian of transformation matrix
H_o ,H_n	Fourier coefficients
k	thermal conductivity

K_v vortex viscosity
j micro-inertia density
J dimensionless parameter characterizes micro-inertia density
M dimensionless microratation
Nu_s local Nusselt numbers
$\overline{Nu}$ average Nusselt numbers
Pr Prandtl number ($=\mu/\rho\alpha$)
Ra Rayleigh number $=\dfrac{\beta g(2a)^3(T_s-T_\infty)}{\nu\alpha}$
t dimensionless time
T temperature
x', y' Cartesian coordinates
Y^* the distance from the tube surface along minor axis $(=\dfrac{y'-b}{\alpha}\mathrm{Ra}^{0.25})$

Greek symbols

α thermal diffusivity
β coefficient of thermal expansion
Δ dimensionless parameter characterizes vortex viscosity
ϕ dimensionless temperature
η, ξ elliptical coordinates
γ spin gradient viscosity
μ viscosity coefficient.
λ dimensionless parameter characterizes spin gradient viscosity
ρ density
ω component of microrotation vector in x', y' plane
τ time
ψ' stream functions
ζ' vorticity

Subscripts

s at the tube surface
∞ at infinite distance from the tube surface

2. The governing equations

Consider a horizontal straight elliptic tube with its major axis vertical and placed in an initially quiescent micropolar fluid at temperature T_∞. The elliptic tube geometry, with major axis of 2a and minor axis of 2b, and coordinates system are shown in Fig. 1. The tube surface temperature is suddenly increased to T_s and accordingly giving the signal to buoyancy driven flow to start. The tube length is assumed long enough to neglect the end effects and to consider the resulting flow and thermal fields to be two dimensional. The effect of temperature variation on fluid properties is considered negligible except for the buoyancy force term in the momentum equation (Boussinesqu approximation). The viscous dissipation and coupling between microrotation and conduction heat flux are neglected. Under these assumptions, the conservation equations of mass, linear momentum , angular momentum and energy in terms of the vorticity, stream function, microrotation and temperature read the following:

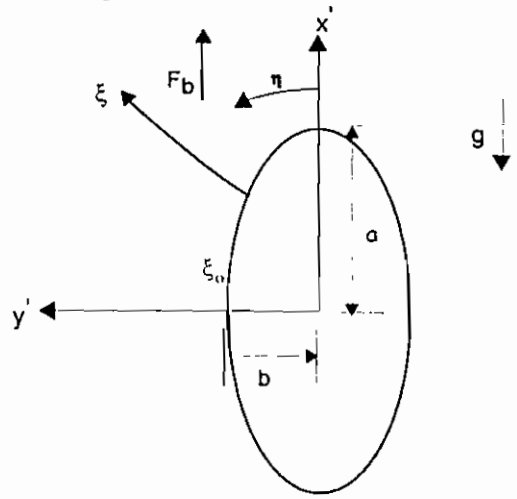

Fig. 1 Tube geometry and coordinate system

$$\frac{\partial\zeta'}{\partial\tau}+\frac{\partial\psi}{\partial y'}\frac{\partial\zeta'}{\partial x'}-\frac{\partial\psi}{\partial x'}\frac{\partial\zeta'}{\partial y'}=\left(\frac{\mu+K_v}{\rho}\right)\nabla^2\zeta'-\frac{K_v}{\rho}\nabla^2\omega+\frac{1}{\rho}\left[\frac{\partial F_{y'}}{\partial x'}-\frac{\partial F_{x'}}{\partial y'}\right] \quad (1)$$

$$\nabla^2\psi'+\zeta'=0 \quad (2)$$

$$\frac{\partial\omega}{\partial\tau}+\frac{\partial\psi'}{\partial y'}\frac{\partial\omega}{\partial x'}-\frac{\partial\psi'}{\partial x'}\frac{\partial\omega}{\partial y'}=\frac{\gamma}{\rho j}\nabla^2\omega+\frac{K_v}{\rho j}(\zeta'-2\omega) \quad (3)$$

$$\frac{\partial T}{\partial \tau}+\frac{\partial \psi'}{\partial y'}\frac{\partial T}{\partial x'}-\frac{\partial \psi'}{\partial x'}\frac{\partial T}{\partial y'}=\frac{k}{\rho c_v}\nabla^2 T \qquad (4)$$

where $\nabla^2=\frac{\partial^2}{\partial x'^2}+\frac{\partial^2}{\partial y'^2}$

τ is the time, ρ is the density, μ is the viscosity coefficient, k is the thermal conductivity and c_v is the specific heat. K_v, j and γ are the vortex viscosity, miero-inertia density and spin-gradient viscosity. ζ' is the vorticity, ψ' is the stream function, T is the temperature and ω is the component of microrotation vector whose direction of rotation is in the x'-y' plane. $F_{y'}=\rho g\beta(T-T_\infty)$ and $F_y=0$ are the components of the buoyancy force , where β is the coefficient of thermal expansion of the fluid.

The boundary conditions are mainly the no-slip, impermeability and no-spin conditions on the tube surface and the stagnant ambient conditions very far away from it.

-on the tube surface

$$\psi'=\frac{\partial \psi'}{\partial x'}=0,\ \frac{\partial \psi'}{\partial y'}=0,\ T=T_s$$

and $\omega=0$ (5a)

-far away from the tube surface

$$\frac{\partial \psi'}{\partial x'}\to 0,\ \frac{\partial \psi'}{\partial y'}\to 0,\ T=T_\infty$$

and $\omega\to 0$ (5b)

Now it is more convenient to use the following dimensionless variables:

$$x=\frac{x'}{a},\quad y=\frac{y'}{a},\quad t=\frac{\tau\alpha}{a^2},\quad \psi=\frac{\psi'}{\alpha},$$

$$\zeta=-\zeta'\frac{a^2}{\alpha},\ M=\frac{a^2\omega}{\alpha},\ \Delta=\frac{K_v}{\mu},\ J=\frac{j}{a^2},$$

$$\lambda=\frac{\gamma}{j\mu}\ \text{and}\quad \phi=\frac{T-T_\infty}{T_s-T_\infty} \qquad (6)$$

Using elliptic coordinates ξ, η such that $x=c\cosh(\xi)\cos(\eta)$, $y=c\sin sh(\xi)\sin(\eta)$, Eqs. (1)-(4) can now be written in terms of the above dimensionless variables as :

$$H\frac{\partial \zeta}{\partial t}=\Pr(1+\Delta)\nabla^2\zeta+\Pr\Delta\nabla^2 M+$$
$$+\frac{cRa\Pr}{8}\left[\cosh\xi\sin\eta\frac{\partial\phi}{\partial\xi}+\sinh\xi\cos\eta\frac{\partial\phi}{\partial\eta}\right]$$
$$+\frac{\partial\psi}{\partial\xi}\frac{\partial\zeta}{\partial\eta}-\frac{\partial\psi}{\partial\eta}\frac{\partial\zeta}{\partial\xi} \qquad (7)$$

$$H\zeta-\nabla^2\psi=0 \qquad (8)$$

$$H\frac{\partial M}{\partial t}=\frac{\partial\psi}{\partial\xi}\frac{\partial M}{\partial\eta}-\frac{\partial\psi}{\partial\eta}\frac{\partial M}{\partial\eta}+\Pr\lambda\nabla^2 M$$
$$-H\Pr\Delta(\zeta+2M)/J \qquad (9)$$

$$H\frac{\partial\phi}{\partial t}=\nabla^2\phi+\frac{\partial\psi}{\partial\xi}\frac{\partial\phi}{\partial\eta}-\frac{\partial\psi}{\partial\eta}\frac{\partial\phi}{\partial\xi} \qquad (10)$$

where $H=c^2(\cosh^2\xi-\cos^2\eta)$ is the Jacobian of transformation, $Ra=g\rho\beta(2a)^3(T_s-T_\infty)/\mu\alpha$ is the Rayleigh number and is the Prandtl number.

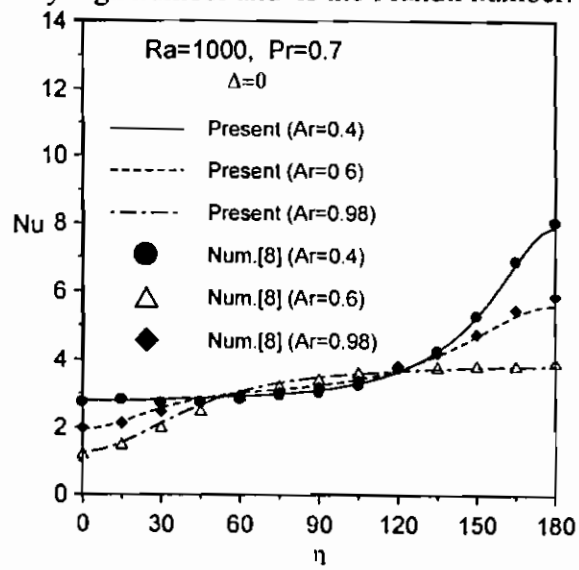

Fig. 2 Local Nu distribution and comparison with the corresponding results of Badr [8] for the case of Newtonian fluid

The boundary conditions Eq. (5) can now be expressed as:

-on the tube surface ($\xi=\xi_w$)

$$\psi=\frac{\partial\psi}{\partial\xi}=0,\quad \frac{\partial\psi}{\partial\eta}=0,\quad M=0$$

and $\phi=1$ (11a)

- very far away from the tube surface

$$(\xi \to \infty), \quad \frac{\partial \psi}{\partial \xi} \to 0, \quad \frac{\partial \psi}{\partial \eta} \to 0, \quad M \to 0$$

$$\text{and} \quad \phi \to 0 \qquad (11b)$$

where $\xi_o = \tanh^{-1}\mathrm{Ar}$ defines the ellipse surface. The temperature of the stagnant fluid around the tube at times $t < 0$ is T_∞ ($\phi = 0$) which is the same as that of the tube surface. At the start of computations ($t = 0$) the tube surface assumes a sudden temperature increase from T_∞ to T_s ($\phi = 1$), and from that moment the time development of both flow and thermal fields commences.

3. The Method of Solution

The method used for solving the governing equations (7)-(10) to obtain the time development of both velocity and temperature fields is based on approximating the stream function, vorticity, microrotation and temperature using Fourier series expansion. The approach is similar to that used by Mahfouz and Badr [17,18]. The stream function ψ, vorticity ζ, microrotation M and temperature ϕ are now approximated as

$$\psi = \sum_{n=1}^{N} f_n(\xi,t)\sin(n\eta) \quad \text{n=1, 2.. N} \qquad (12a)$$

$$\zeta = \sum_{n=1}^{N} g_n(\xi,t)\sin(n\eta) \qquad (12b)$$

$$M = \sum_{n=1}^{N} r_n(\xi,t)\sin(n\eta) \qquad (12c)$$

$$\phi = H_o/2 + \sum H_n(\xi,\eta)\cos(n\eta) \qquad (12d)$$

where N is the number of terms in the Fourier series. The functions f_n, g_n, r_n, H_o and H_n are Fourier coefficients and all are dependent on ξ and t and can be deduced similarly to those in Mahfouz and Badr [17]. The rest of the details of the method of solution is more or less similar to that in Refs. [16-19] and will not be repeated here for the sake of brevity.

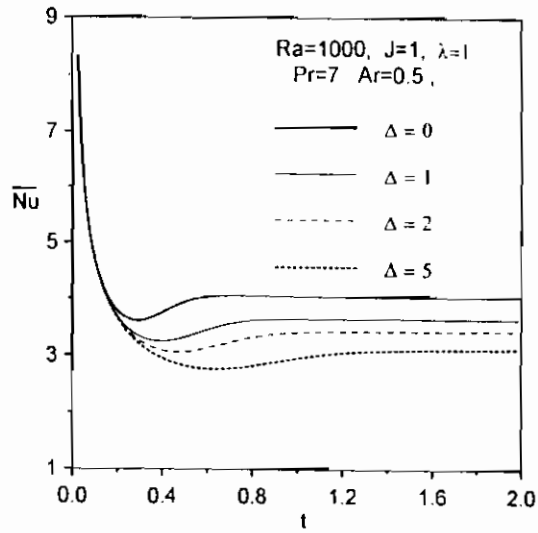

Fig. 3 The time development of $\overline{Nu}$

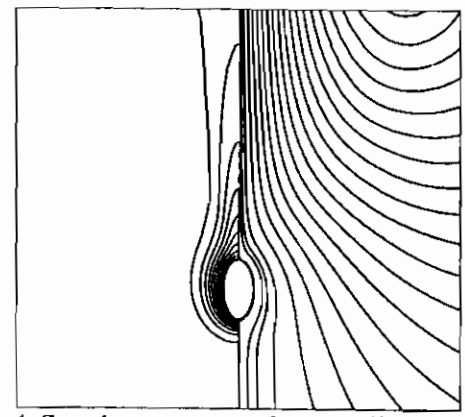

Fig 4 Steady patterns of streamlines (right) and isotherms (left) for case of Ra=1000, $\lambda = 1$, $\Delta = 1$ and J=1.

The heat transfer results are usually expressed in terms of Nusselt number. The local surface Nusselt number is defined as

$$Nu = \frac{2a\dot{q}}{k(T_s - T_\infty)} \qquad (13)$$

where $\dot{q} = -k(\partial T/\partial s_n)_{\xi_o}$, $\dot{q}$ is the rate of heat transfer per unit area , S_n is the normal direction to the tube surface. From the above definitions the Nu can be expressed in terms of Fourier coefficients H_0 and H_n as

$$Nu = \frac{-1}{\sqrt{H_s}}\left[\frac{\partial H_0}{\partial \xi} + 2\sum_{n=1}^{n=N}\frac{\partial H_n}{\partial \xi}\cos(n\eta)\right]_s \qquad (14)$$

The average surface Nusselt number can be expressed as

$$\overline{Nu} = \frac{1}{P}\int_0^P Nu\, dP = -\frac{2\pi a}{P}\left(\frac{\partial H_0}{\partial \xi}\right)_{\xi=\xi_s} \qquad (15)$$

where P is the perimeter of the elliptic section.

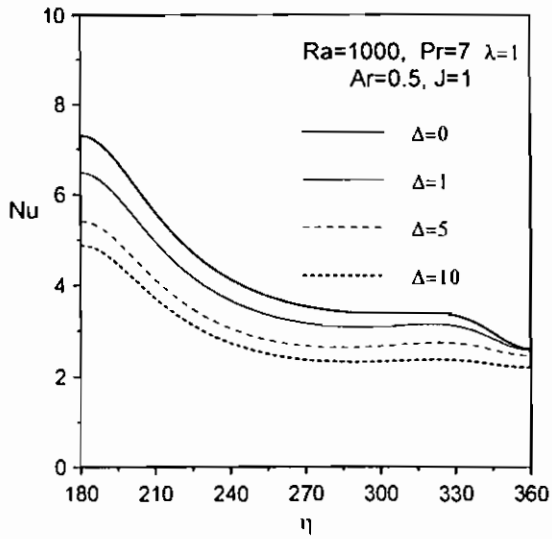

Fig. 5 Steady state local Nusselt number distibution

4. Results and Discussion

In order to solve the discretized governing equations along with the boundary conditions, a series of runs has been carried out on the computer program that has been developed and tailored for the present problem. The program has been fed with the main influencing controlling parameters that affect both flow and thermal fields. These parameters, as can be seen from the governing equations, are Rayleigh number Ra, Prandtl number Pr, axis ratio Ar and the material parameters λ, Δ and J. For the sake of brevity only the effect of Ra, Δ and J are considered while Pr, and λ are fixed at 7 and 1, respectively. The calculations are carried out in part for the case of elliptic tube of axis ratio of 0.5 and in part for the special case of vertical plate where axis ratio approaches zero. The Rayleigh number Ra, is considered in its moderate range up to 10^4. The material parameter Δ, which characterizes vortex viscosity is considered in the range from 0 to 10 while the material parameter J, which characterizes micro-inertia density, is considered in the range from 0.1 to 10. These values for material parameters satisfy the thermodynamics restrictions given by Eringen [2]. The values considered here for controlling parameters may be changed whenever comparison with others is concerned.

4.1 Accuracy of the numerical solution

The numerical simulations were carried out only after validating the method of solution and numerical technique. The first problem considered for validation was the case of natural convection from circular cylinder placed in a micropolar fluid. The problem has been separately investigated by Mahfouz [19]. In that work the author used the same method of solution in handling the full governing equations which were written in polar coordinates. To compare the present results with those for circular cylinder, the circular geometry has to be generated from the elliptic geometry by setting axis ratio to one. Setting axis ratio to one leads to overflow errors in the present computer code. To circumvent this problem the axis ratio was set to 0.998 which is very close to one. The comparisons were carried out after matching the corresponding controlling parameters and boundary conditions. The test runs have produced results (not shown here) very close or even identical to those in Mahfouz [19]. This confidently ruled out any possibility of errors in handling either the governing equations or their transformation to elliptic coordinates and confirmed the accuracy of the method of solution as well.

The second problem considered for comparison was the case of natural convection from elliptic tube placed in a Newtonian fluid with its major axis vertical considered by Badr [8]. The present results for distribution of the steady state local Nusselt number along the elliptic tube surface at Ra=1000, Pr=0.7 and at three axis

ratios, namely, 0.4, 0.6 and 0.98 are shown in Fig. 2 together with the corresponding numerical results of Badr. It can be seen from the figure that the present results are in very good agreement with those of Badr for the three axis ratios with maximum difference not exceeding 3 %. The above comparisons and the comparisons that will be provided wherever convenient, confirm the high accuracy of the numerical solution.

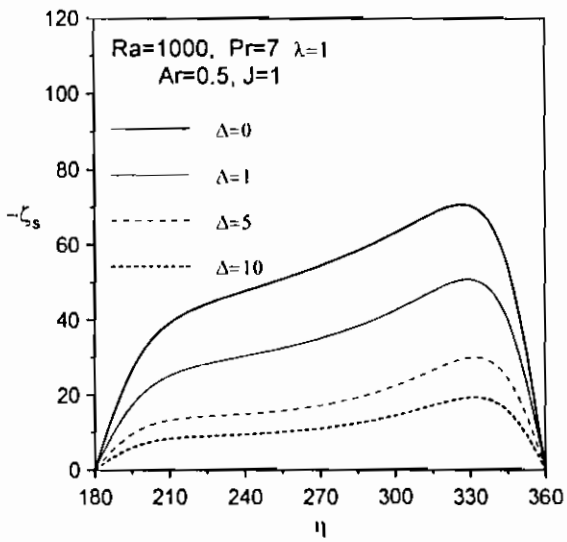

Fig. 6 Steady state surface vorticity distibution

4.2 Results for elliptic tube of Ar=0.5

Fig. 3 shows the time variation of surface average Nusselt number $\overline{Nu}$, for the case of Ra=1000, and at different values of dimensionless vortex viscosity $\Delta = 0$, 1, 2 and 5. The figure clearly shows that the general variation of $\overline{Nu}$ is similar to that for Newtonian fluids ($\Delta = 0$). That is $\overline{Nu}$ evolves in a sequence of pure conductive, transient convective and steady convective processes. The pure conductive process prevails immediately after the tube surface temperature is increased. The high temperature gradient established near the tube surface results in high heat flux and so high values of $\overline{Nu}$. In this early time stages and as a result of quick developing of thermal boundary layer a quick decrease in $\overline{Nu}$ occurs, reaching to a minimum value at a certain short time. Beyond this time, the buoyancy force becomes more effective, causing transient convective process. This transition as shown in the figure takes a form of overshoot in $\overline{Nu}$. Such a phenomenon has been depicted and further explained for the relevant natural convection problems [19-23]. At late times the convective process gradually prevails with steady rates of heat transfer and so steady $\overline{Nu}$ gradually approach.

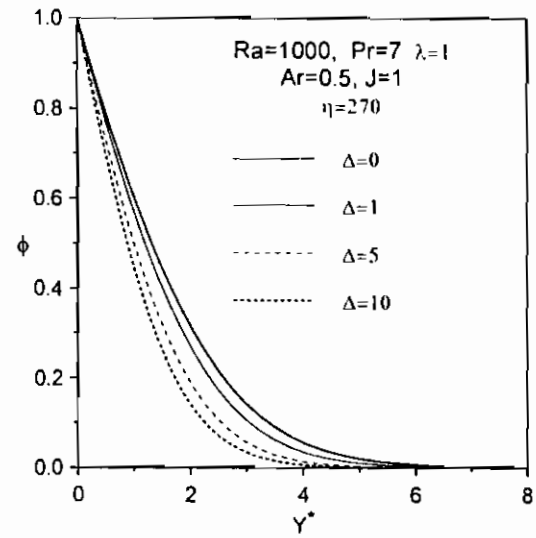

Fig. 7 Steady state temperature variation along minor axis of the tube

In addition, Fig. 3 shows that the late time or the steady $\overline{Nu}$ in the case of micropolar fluids ($\Delta = 1, 2, 5$) is lower than that for Newtonian fluid ($\Delta=0$). This decrease may be attributed, as explained in Hsu et al. [24], to the increase of the flow viscosity as a result of vortex viscosity. Increasing of flow viscosity weakens the flow convection currents and increases the thickness of the thermal boundary layer which in turn decreases heat transfer rates (and so $\overline{Nu}$). Since the conduction mode of heat transfer is predominant in the initial stages the vortex viscosity has no role and $\overline{Nu}$ for micropolar fluid and that for Newtonian fluid are identical. As the

convection domination mode starts the vortex viscosity of micropolar fluid enhances the flow viscosity and so decreases the heat transfer rate. The larger the value of Δ the larger the flow viscosity and the lower the value of steady state $\overline{Nu}$.

A typical example for steady flow and thermal fields at late time is shown in Fig. 4. The figure shows the flow field, in terms of streamlines, and the thermal field, in terms of isotherms, for the case of Ra=1000, $\lambda = 1$, $\Delta = 1$ and J=1. Since these fields are symmetrical about the vertical axis, only one half of each field is considered. The figure shows condensed isotherms close the bottommost point which declares high temperature gradient and so high heat rate in that region while the streamlines are more condensed close to the topmost region declaring high velocity and so high surface vorticity in that region.

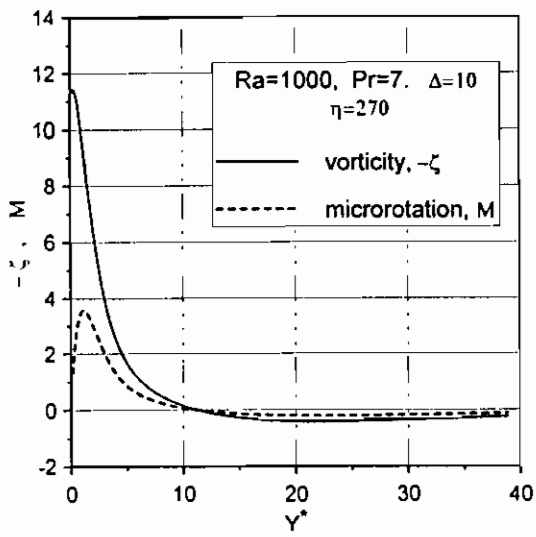

Fig. 8 Steady state vorticity and microrotation variation along minor axis

The steady state values of $\overline{Nu}$ for the cases considered in this study are listed in Table 1. The Table shows the effect of Rayleigh number Ra, and the material parameters Δ and J of micropolar fluid on the steady state average Nusselt number, $\overline{Nu}$. It can be seen that the effect of Ra on steady state $\overline{Nu}$ is quite clear, that is at any fixed value of fluid material parameters as Ra increases the $\overline{Nu}$ increases. This is quite expected since increasing of Ra leads to increasing of convection currents and so increasing the heat transfer rate. Also, it can be seen that as the material parameter Δ increases at any fixed value of Ra the $\overline{Nu}$ decreases. The table also shows that at fixed values of Ra, and Δ the material parameter J has almost negligible effects on the $\overline{Nu}$ in the range considered for the parameters. So, it can be inferred from Table 1 that the vortex viscosity is the most influencing material parameter on both flow and thermal fields.

Table 1 Effect of Ra and material parameters Δ and J on steady state average Nusselt number.

Ar	Ra	Δ	J	$\overline{Nu}$
0.5	10^3	------	------	4.03
		1	0.1	3.66
		5	0.1	3.23
		10	0.1	2.98
		1	1	3.63
		5	1	3.11
		10	1	2.87
		1	10	3.65
		5	10	3.08
		10	10	2.78
	10^4	-----	------	6.55
		1	0.1	5.79
		5	0.1	4.93
		10	0.1	4.56
		1	1	5.77
		5	1	4.79
		10	1	4.38
		1	10	5.79
		5	10	4.81
		10	10	4.35

------ refers to a Newtonian fluid

The steady state local Nusselt number distributions at Ra =1000 and at different values of dimensionless vortex viscosity are

shown in Fig. 5. Since the thermal field is symmetrical about the vertical axis, only one-half of Nu distribution is shown. It can be seen that Nu is maximum at the bottommost point $\eta = 180$ and minimum at the topmost point $\eta = 360$ for all values of Δ, though it is smaller for bigger values of Δ. It can be also observed that as η increases from the bottommost point toward the topmost point, the Nu decreases till almost point ($\eta = 240$), and keeps almost constant up to point ($\eta = 300$) then decreases, reaching its minimum at the topmost point. The figure clearly shows that, at any surface point Nu decreases as Δ increases which accordingly means decreasing of steady $\overline{Nu}$ as Δ increases as shown in Table 1.

Fig. 6 shows the surface vorticity distribution for the same above case and for the same half of the surface. The vorticity distribution over the other half would have exactly the same values but with negative signs. The figure shows that the surface vorticity at any fixed value of Δ increases rapidly from zero at bottommost point ($\eta = 180$) up to $\eta = 210$. Then the surface vorticity continues increasing but with smaller rate till reaching its maximum value at almost $\eta = 330$ and then sharply decreases to zero at topmost point ($\eta = 360$). The figure also shows that as Δ increase the surface vorticity decreases at all points of the tube surface . Decreasing of surface vorticity with increasing of Δ reflects the decrease of velocity gradients at the tube surface which reflects in turn the weakness in the flow convection currents. The weaker the flow currents the smaller the heat flux (and so Nu).

Fig. 7 shows the temperature variation along the extension of the ellipse minor axis ($\eta = 270$) for the case of Ra = 1000, J=1 and at different values of dimensionless vortex viscosity, Δ. It can be seen that the fluid temperature decays with distance from tube surface till it reaches eventually the stagnant fluid temperature (i.e $\phi = 0$). Also. the figure clearly shows that as Δ increases the temperature gradient at the tube surface decreases and accordingly local heat transfer decreases which in turn means a decrease in Nu as can be seen in Fig. 5.

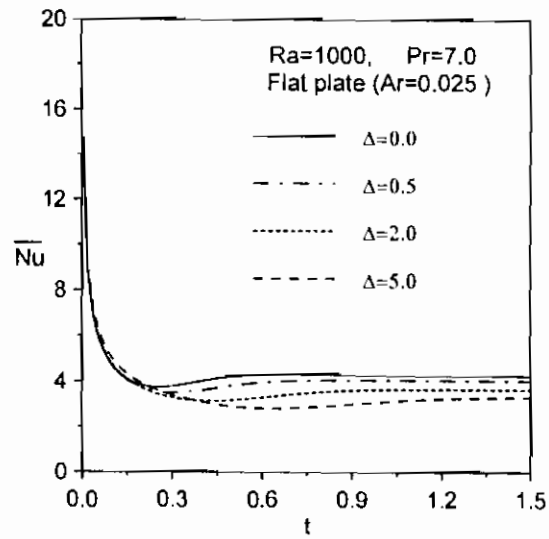

Fig. 9 The time development of $\overline{Nu}$ in case of vertical flat plate

Table 2 Effect of Ra, Δ and J on steady state $\overline{Nu}$ for vertical flat plate

Ra	Δ	J	$\overline{Nu}$
1000	----	----	4.232
	0.5	0.1	4.021
	1	0.1	3.874
	2	0.1	3.694
	5	0.1	3.407
	0.5	1	4.021
	1	1	3.859
	2	1	3.643
	5	1	3.304
	0.5	10	4.030
	1.0	10	3.876
	2.0	10	3.662
	5.0	10	3.281

Fig. 8 shows the steady state variation of both vorticity and microrotation along the minor axis of the tube for the case of Ra=1000, J=1 and Δ=10. The figure

shows that the values of both vorticity and microrotation are significant in the nearby region of the tube (in the boundary layer region) and almost negligible elsewhere along the axis extension. It can also be inferred that the direction of rotation of both mean flow and fluid elements along the minor axis is the same. The mean flow rotation is represented by vorticity while fluid elements rotation is represented by the microrotation. Moreover, the point of zero vorticity and zero microrotation or the point at which the mean flow and fluid elements change direction of rotaion is the same for both of them. The consisitency of this result with the logical exepectation from one side supports the valdity of the micropolar fluid model developed by Eringin [1] and from the other side supports the validaty and accuracy of the present numerical technique.

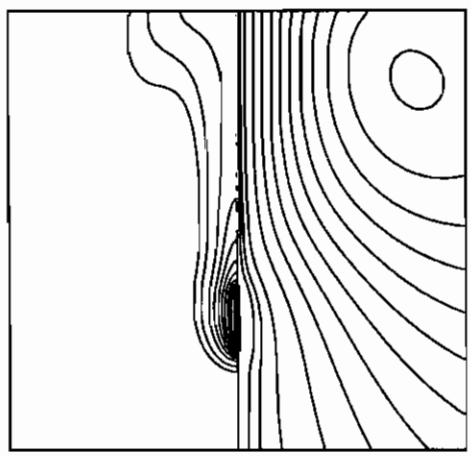

Fig 10 Steady patterns of streamlines (right) and isotherms (left) for case of Ra=1000, $\lambda = 1$, $\Delta = 5$ and J=1.

4.3 Results for vertical flat plate

In the following the natural convection from vertical plate is considered. This case can be obtained by setting axis ratio Ar, to zero in the present calculation. Setting Ar=0, though produces no errors in computer code, means that the vertical plate has no thickness which physically unrealistic. The flat plate must have a thickness, no matter how small it is, therefore, in the present calculation the axis ratio of 0.025 has been considered as a good approximation for the flat plate case. In that regard Raithby and Hollands [4] have pointed out that near flat plate limit Ar < 0.1 there was almost no dependence of heat transfer on axis ratio.

Fig. 9 shows the time variation of $\overline{Nu}$ for the case of vertical flat plate. Generally, it can be inferred from the figure that the time development of both flow and thermal fields in the case of vertical plate is more or less similar to that for the case of Ar=0.5. That is immediately after the temperature of the plate surface is raised, a temperature gradient is established within the fluid layer adjacent to the plate surface, causing predomination of conduction mode of heat transfer with higher rates of heat transfer (and so $\overline{Nu}$) . At this early time stages the newborn buoyancy force causes the commencement of fluid motion with rapid increase of thermal layer and so rapid decrease in $\overline{Nu}$. As the time goes, the buoyancy–induced motion intensifies with gradual transition to convection mode domination heat transfer. This transition takes a form of overshoot in heat transfer (i,e in $\overline{Nu}$). At late times, the convection mode dominates and the flow and thermal fields in the vicinity of the plate surface gradually tend to be almost steady. The steadiness in the nearby flow and thermal fields at late time leads to steady rates of heat transfer. In addition, the figure clearly shows that as Δ increases the late time or steady state value for $\overline{Nu}$ decreases.

The steady state values for average surface Nusselt number for the case of vertical flat plate in case of microloar fluid are listed in Table 2 for the selected value of Ra of 1000. A quick inspection of Table 2 and Table 1 for Ra=1000 shows that for the same material parameters the $\overline{Nu}$ values for flat plate are higher than those for elliptic tubes, giving an indication of increasing $\overline{Nu}$ as Ar decreases. Decreasing of $\overline{Nu}$ as Ar decreases has been reported in previous works for Newtonian fluids (see Badr [8]).

Table 2 again confirms the fact that as Δ increases the Nu decreases and confirms also that the parameter J has insignificant effect on heat transfer as compared with the parameter Δ.

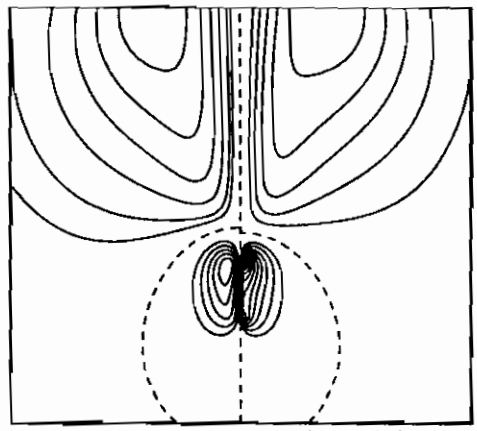

Fig 11 Steady patterns of vorticity (right) and microrotaion (left) patterns for case of Ra=1000, $\lambda = 1$, $\Delta = 5$ and J=1.

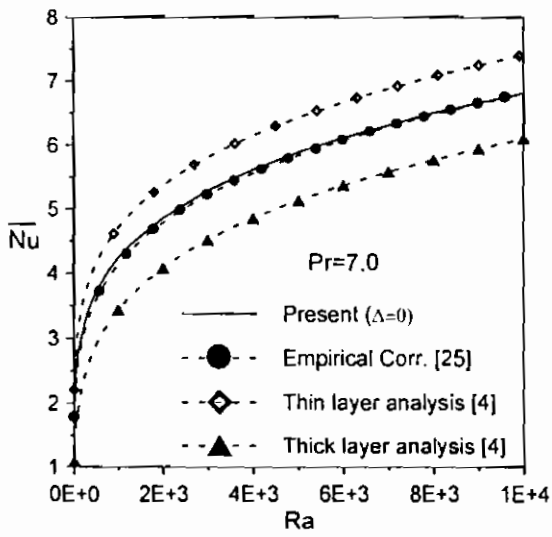

Fig. 12 Variation of $\overline{Nu}$ with Ra and comparison with the empirical correlation of [4] and [25]

The flow and thermal fields in case of free convection from the flat plate at late time is shown in Fig. 10. The figure shows the flow field, in terms of streamlines, and the thermal field, in terms of isotherms, for the case of Ra=1000, $\lambda = 1$, $\Delta = 5$ and J=1. The figure shows that these distributions are generally similar to those for Newtonian fluids. Also it can be seen from the figure that the stream lines are condensed near the top of the plate which means higher flow velocity and so higher convection in that region. The vorticity and microrotation patterns for the same case and at the same time are shown in Fig. 11. The figure clearly shows that both patterns are very similar with even zero vorticity and zero microrotation contours (dashed lines) are almost identical.

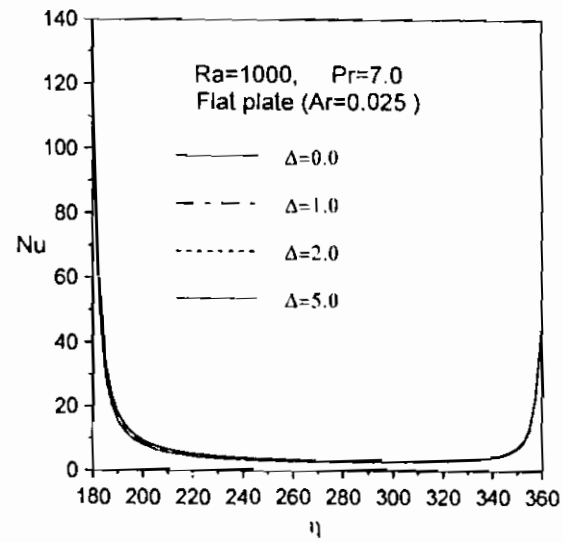

Fig. 13 Steady state local Nusselt number distibution

Shown in Fig. 12 are the present results for steady state average Nusselt number variation with Rayleigh number, Ra for the case of natural convection from a vertical plate placed in Newtonian fluid (Δ=0). Shown also in the same figure is the empirical correlation proposed by Churchill and chu [25]. For laminar flow range the correlation takes the form:

$$\overline{Nu} = 0.68 + \frac{0.67 Ra^{0.25}}{\left[1 + (0.492/\mathrm{Pr})^{9/16}\right]^{4/9}} \qquad (16)$$

The figure shows an excellent agreement between the present results and the correlation (16). The approximate solutions of Raithby and Hollands [4] given for

18. Mahfouz, F. M., and Badr, H. M., 2000, Flow structure in the wake of a rotationally oscillating cylinder, ASME J. of Fluids Engineering, 122, pp. 290-301.
19. Mahfouz, F. M., 2003, Transient free convection from a horizontal cylinder placed in a micropolar fluid, Heat and Mass Transfer, 39, pp 455-462.
20. Parsons Jr., J. R. and Mullgan J. C., 1978, Transient free convection from a suddenly heated horizontal wire, ASME J. of Heat Transfer, 100, pp. 423-428.
21. Jia, H. and Gogos, G., 1996, Transient laminar natural convection heat transfer from isothermal spheres, Numerical Heat Transfer, Part A 29, pp. 83-101.
22. Wang, P., Kahawita R. and Nguyen D. L., 1991, Transient laminar convection from horizontal cylinders, Int J. Heat Mas Transfer, 34(8) pp. 1429-1442.
23. Badr, H. .M., 1987 Heat transfer in transient buoyancy driven flow adjacent to a horizontal rod. Int. J Heat and Mass Transfer 30, pp. 1990-2012
24. Hsu, T., Hsu, P. and Tsai, S., 1997, Natural convection of micropolar fluids in an enclosure with heat sources, Int. J. of Heat and Mass Transfer, 40(17), pp. 4239-4249.
25. Churchill, S. W. and Chu, H. S., 1975, Correlating equations for laminar and turbulent free convection from a vertical plate, Int. J. of Heat and Mass Transfer, 18, pp. 1323-1329.